Review of Scientific Instruments

Portable (handheld) clinical device for quantitative spectroscopy of skin, utilizing spatial frequency domain reflectance techniques

Cite as: Rev. Sci. Instrum. **88**, 094302 (2017); https://doi.org/10.1063/1.5001075
Submitted: 25 April 2017 • Accepted: 21 August 2017 • Published Online: 07 September 2017

Rolf B. Saager, An N. Dang, Samantha S. Huang, et al.

AIP Publishing

Portable (handheld) clinical device for quantitative spectroscopy of skin, utilizing spatial frequency domain reflectance techniques

Rolf B. Saager,[1,a)] An N. Dang,[1] Samantha S. Huang,[1] Kristen M. Kelly,[1,2] and Anthony J. Durkin[1]

[1]*Beckman Laser Institute and Medical Clinic, University of California, Irvine, 1002 Health Sciences Road East, Irvine, California 92612, USA*

[2]*Department of Dermatology, University of California, Irvine, 118 Medical Surge 1, Irvine, California 92697, USA*

(Received 25 April 2017; accepted 21 August 2017; published online 7 September 2017)

Spatial Frequency Domain Spectroscopy (SFDS) is a technique for quantifying *in-vivo* tissue optical properties. SFDS employs structured light patterns that are projected onto tissues using a spatial light modulator, such as a digital micromirror device. In combination with appropriate models of light propagation, this technique can be used to quantify tissue optical properties (absorption, μ_a, and scattering, μ_s', coefficients) and chromophore concentrations. Here we present a handheld implementation of an SFDS device that employs line (one dimensional) imaging. This instrument can measure 1088 spatial locations that span a 3 cm line as opposed to our original benchtop SFDS system that only collects a single 1 mm diameter spot. This imager, however, retains the spectral resolution (~1 nm) and range (450–1000 nm) of our original benchtop SFDS device. In the context of homogeneous turbid media, we demonstrate that this new system matches the spectral response of our original system to within 1% across a typical range of spatial frequencies (0-0.35 mm^{-1}). With the new form factor, the device has tremendously improved mobility and portability, allowing for greater ease of use in a clinical setting. A smaller size also enables access to different tissue locations, which increases the flexibility of the device. The design of this portable system not only enables SFDS to be used in clinical settings but also enables visualization of properties of layered tissues such as skin. *Published by AIP Publishing.* [http://dx.doi.org/10.1063/1.5001075]

I. INTRODUCTION

Biological tissues, such as skin, contain a variety of physiological properties that can be probed non-invasively by light. Chemical constituents present in tissues, such as oxygenated and deoxygenated hemoglobin, melanin, lipids, carotenoids, and water, can absorb light at differential energies, producing a distinct spectral signature across both visible and near infrared regimes. Light can also elastically scatter off of subcellular (e.g., nuclei and mitochondria) and extra-cellular (e.g., collagen) structures, where the size and orientation of these structures can influence the tortuous paths photons travel through the tissue. Techniques based on models of light transport in tissues have been developed to extract and isolate the effects of tissue absorption and scattering and thereby quantify functional parameters (hemoglobin concentrations, melanin concentration, etc.)[1] and gain insight of the bulk structural organization of the tissue,[2] respectively.

These techniques may be deployed in a variety of reflectance based measurement geometries ranging from fiber probe-based point spectroscopy to wide-field imaging approaches, while also utilizing a number of illumination/detection schemes to exploit temporal and/or spatial responses from light interactions with tissues.[3–8] One of the significant challenges in terms of these approaches is related to the accurate interpretation of measurements obtained from the tissue that is highly structured and/or heterogeneous in depth. This is of particular concern for skin, since melanin may only be present in proximity to the epidermis, often within the most superficial 100 μm of skin. For example, the melanin associated with normal pigmented nevi has been reported to lead to errors in measurement of oxygen saturation within the dermis lying beneath these lesions. This is a consequence of inadequate accounting for superficial melanin.[9] Similarly, in normal skin, the average local tissue oxygen saturation has been shown to trend inversely with the amount of melanin in the skin as assessed across different skin colors (corresponding to pigmentation differences spanning Fitzpatrick types I-V). This indicates that the presence of melanin, if incompletely accounted for, can directly influence the interpretation of spectral signatures related to blood.[10,11] Several methods have since been proposed and developed to address this issue in skin. Among these are multi-layer models to describe light transport within structured tissues[12–15] and semi-empirical methods to minimize cross talk between depth-specific chromophores.[16]

A. Benchtop spatial frequency domain spectroscopy (SFDS) instrument

In order to solve some of these problems, our group has developed a novel quantitative spectroscopic method using a combination of projected structured patterns that illuminate the tissue and enables exploitation of the differential response in scattering and absorbing properties over a wavelength range that spans visible and near infrared portions of

a)rsaager@uci.edu

the spectrum.[17] This approach, which is referred to as Spatial Frequency Domain Spectroscopy (SFDS), interrogates tissues with a series of sinusoidal intensity patterns and detects the remitted light over a range of 450-1050 nm with ~1 nm spectral resolution.

A diagram of our benchtop SFDS instrument (also known as spatially modulated quantitative spectroscopy, SMoQS) showing its typical configuration used in several previous *in vivo* investigations is illustrated in Fig. 1.[17–20]

A 100 W Quartz-Tungsten-Halogen (QTH) light source (Moritex, MHF-D100LR) is coupled to a digital micro-mirror device—DMD (Alligator XGA DMD module, GFMesstechnik, Berlin, Germany) in order to project structured light patterns with spatial frequencies from 0 to 0.3 mm^{-1}. The projection field of view (FOV) for this system is 22 × 17 mm. The distal end of a 1 mm core optical fiber (TechSpec, NA 0.39, Thorlabs, Inc.) is imaged at the center of the projection field of view (1:1 magnification). This defines the collection area of interest, 1 mm, and is an example of what we refer to as point spectroscopy. The light collected by this fiber is delivered to a spectrometer (Oriel 77480) enabling measurements over the range 450–1000 nm. Crossed 2-in. diameter wire-grid polarizing filters are used to reject specular reflection from the surface of the sample. The polarizer is inserted between the DMD and projection optics, and the analyzer is located between the fiber and collection optics.

SFDS can quantify the absorption and scattering properties in both visible and near-infrared regimes and we can employ this to estimate the depth each wavelength interrogates in tissues.[21,22] This allows SFDS to interpret every part of the measured spectrum in terms of the volume of tissues it interrogates. This is uniquely advantageous, as (1) skin is highly structured, consisting of epidermis (~100 μm) and dermis (~millimeters), and (2) the typical depth penetrance of visible light is on the order of 100's microns, while near-infrared is on the order of millimeters. Based on this, we have developed a semi-empirical method to estimate chromophore concentrations in skin as a function of depth via a two-layer model that leverages the differential depth penetrance between visible and near infrared light.[19] This model has been validated *in vivo* in terms of its ability to estimate melanin concentration and epidermal thickness across a wide range of skin pigmentation (skin types I-VI on the Fitzpatrick scale).[20] We have also validated the ability of SFDS to minimize the role of melanin in terms of corrupting the estimation of underlying chromophores oxy- and deoxyhemoglobin, which are associated with hemodynamics.[18]

While the benchtop configuration illustrated in Fig. 1 has been useful for the development and validation of quantitative layered model approaches that can address the depth specific structures in tissues such as skin, that device can acquire only a single, 1 mm diameter spot at a time, enabling limited lateral spatial resolution. Furthermore, the system is large, cumbersome, and difficult to transport (including misalignment). For those reasons, *in vivo* data collection has been typically relegated to the proof of principle studies rather than engaging in more translational studies to address specific clinical challenges, such as those that might enable early melanoma screening. To that end, we present a new compact instrument design that exploits the quantitative spectroscopic attributes of previous SFDS *in vivo* studies however executes this technique through a portable, handheld imaging system that also introduces spatial imaging capabilities along a single lateral dimension.

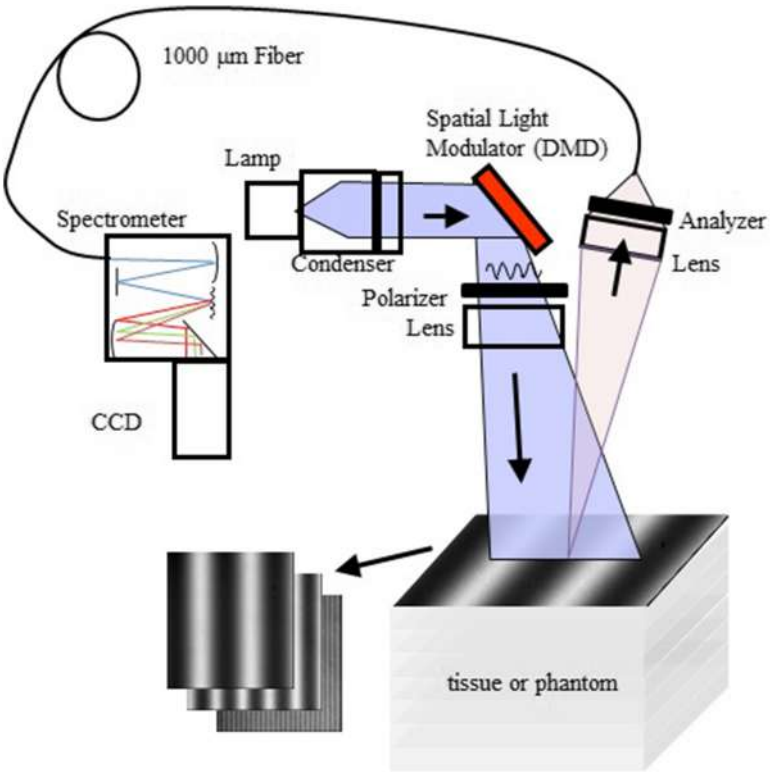

FIG. 1. System diagram for benchtop SFDS instrument used in previous experiments. Note that light is collected only from a 1 mm diameter spot centered within the illuminated 22 × 17 mm area.

In this paper, we describe the design and fabrication of this new instrument. The performance of this device will be compared to that of the benchtop, point-spectroscopy system in terms of (1) independently characterized tissue simulating phantoms to validate the accuracy and fidelity of the SFDS system and (2) an *in vivo* measurement of a benign pigmented lesion to illustrate the application of this technique in a clinical context.

II. INSTRUMENT DEVELOPMENT

A. System design criteria

The primary emphasis on the design of this SFDS imaging system is that it (1) is compact and easily portable and (2) collects data along one spatial dimension (line imaging spectroscopy as opposed to single "point" spectroscopy), while (3) maintains the spectral range and resolution of our the benchtop, system (Fig. 1). These three objectives translate to a number of specific design criteria when considering the selection of hardware components and the device assembly.

As clinical space is often limited and distributed across a number of examination rooms, our device is designed to possess a small footprint and be portable such that it can be easily moved between adjacent clinical exam rooms. To that end, our design considers compact components, such as commercial micro-projectors, miniature, fixed slit imaging spectrographs, coupled light-sources, and laptops to operate the device. These components can then be either integrated into a handheld imaging head or stored within a small cart.

Melanoma lesions are often spatially heterogeneous in terms of the distribution of tumor cells within a suspect pigmented area of tissues (and occasionally non-pigmented regions, amelanotic melanoma). It is, therefore, highly desirable for a spectroscopic instrument design to be able to collect spatially distributed data from a tissue region of interest in order to assess the relative distribution and compositional variance from both the suspect lesion and adjacent tissue. To this end, the design presented here employs a line imaging spectrometer that enables collection of data from a 30 mm line at the opening of the nose cone (nose cones will be described in Sec. II B 4).

Spectral resolution and range are also important for SFDS as the technology was expressly developed as a method to characterize the spectral properties (and chromophore concentrations) of *in-vivo* tissues. By spanning visible and near infrared ranges with ~1 nm resolution, SFDS is capable of quantifying both tissue scattering and absorption properties without any *a priori* assumptions of the chromophores present in tissues. This enables documentation of characteristic spectral features of normal tissues as well as identifying potential alterations in spectral components due to disease states.

B. Hardware description

1. Illumination/projection unit

In order to provide broadband illumination for the device described here, we have selected a 150 W Quartz Tungsten Halogen light source (Model 21DC, Techniquip, Pleasanton, CA). While this unit is relatively large (18 × 20 × 10.5 cm), it is designed to couple light into a fiber bundle or liquid light guide. This unit is stored on a compact cart and a 2 m long liquid light guide (77639, Newport, Irvine, CA) is employed to deliver the broadband light to the handheld imaging head.

An Optoma pico-projector (PK320, Optoma, Fremont, CA) is employed for our compact projection unit as it uses a digital mirco-mirror device (DMD), which has been the basis of the majority of SFDS instruments.[7,17,23–26] It is an off-the-shelf commercial "pocket projector" with physical dimensions of 3 × 8 × 12 cm and a cost of ~$150-300. In contrast, our benchtop system uses a research-grade DMD-based projection unit (Alligator XGA DMD module, GFMesstechnik, Berlin, Germany) with dimensions of 12 × 7 × 20 cm and a cost of ~$10-15 k.

As a commercial product intended for projecting computer screens over large distances and fields of view, the Optoma projector requires several modifications before it can be used in a SFDS instrument. The projector uses red, blue, and green (RGB) light-emitting diodes (LEDs), while SFDS, for our skin investigations, requires broadband illumination spanning 450–970 nm in order to enable quantification of melanin, hemoglobin, and water fraction. In order to convert the projector to employ broadband illumination, the red and green LEDs were removed from the projector along with their respective dichroic mirrors (Fig. 2). (The blue LED is covered/blocked, unused as part of the light source, but kept in the system because it also serves as an electrical interlock that enables the system firmware to operate.) A slot has been carved out of the plastic housing through which we introduce a liquid light guide for the broadband light source and secure it into the position formerly occupied by the red LED. With this modification to the optical light path, broadband illumination is directed through the remaining optical components of the projector.

The second modification to the projector addresses the working distance and field of view of the projection optics that are native to the Optoma. Our objective is to project sinusoidal intensity patterns over a ~40 mm field of view. This is because the pigmented lesions that we are interested in imaging typically range 5-30 mm in diameter.[27] Given that the instrument is designed to be handheld, we also want to limit the distance between the device and the tissue of interest. Inserting a 100 mm focal length field lens at the distal end of the projection lens system resulted in a 39 mm field of view and a working distance of 65 mm.

2. Detection unit

A compact slit-imaging spectrometer (ImgSpec, BaySpec, Inc., San Jose, CA) was chosen to provide spectral dispersion of light collected from a line transecting the tissue region of interest. The BaySpec device is a ruggedized unit with dimensions of ~22 × 6 × 6 cm and weighs approximately 5 lb. It uses a transmission grating that covers a range of 400-1100 nm and a large format (1 in.) CMOS sensor as the detector. With an entrance slit of 14.2 mm × 30 μm, the resulting spectral resolution on the 2048 × 1088 pixel sensor is ~1 nm. Relative

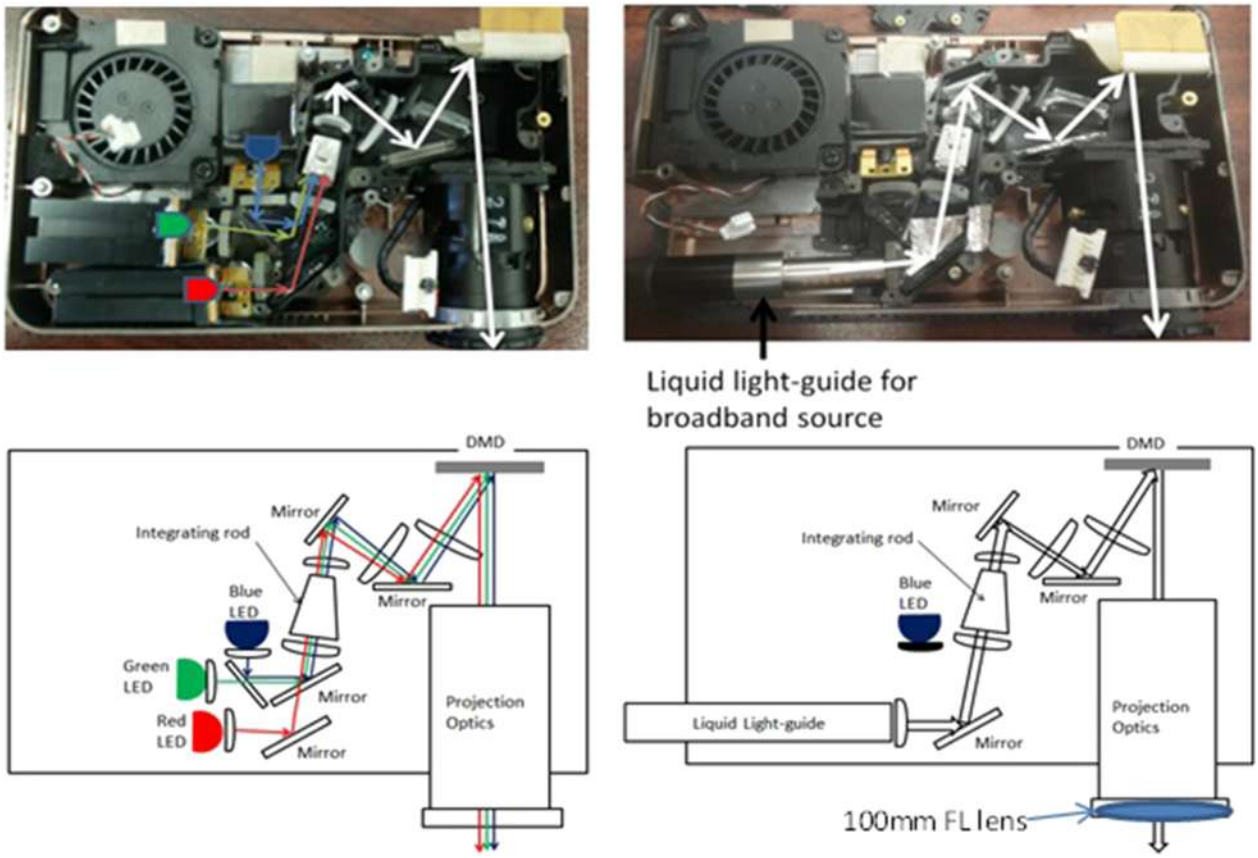

FIG. 2. Modification of the Optoma pico-projector. Left: Image (top) and schematic (bottom) of the optical path of the original projector. Right: Image and schematic of the modified optical path. Here the red and green LEDS are removed. The blue LED also serves as a system interlock, so it was left in place but blocked by black electrical tape. The dichroic mirror that combines the green and blue LEDs with the red LED was removed and a liquid light guide, delivering broadband light, was inserted into the red LED light path.

to the spectrometer used in the benchtop (Fig. 1) system (Oriel 4770, Newport, Irvine, CA), this compact unit shares an equivalent spectral range and resolution. The BaySpec spectrometer, however, can resolve 1088 spatial locations simultaneously by imaging the vertical dimension of the 14.2 mm tall slit, while our benchtop system relies on an Oriel spectrometer that is limited to data collection from a single 1 mm diameter spatial location.

Integrating the line-imaging spectrometer into a handheld system with the modified projector also required custom mounting components and minor modifications. To achieve a target field of view (FOV) and working distance of ~30 mm and 150 mm, respectively, via the 35 mm visible and near infrared (Vis/NIR) fixed focal length C-mount lens (#67-716, Edmund Optics) provided with the unit, a 1 mm brass spacer was added to the C-mount thread to modify back focal plane between entrance slit and lens system (Fig. 3).

3. Handheld imager assembly

This portable system was designed with two particular sub-components in mind: a handheld imaging head and a small, mobile computer cart [not shown, dimensions: 45 cm (W) × 56 cm (L) × 76 cm (H)] to house the light. There is a 2 m umbilical that connects all power, universal serial bus (USB) and optical cables between the cart and imager.

Figure 3 depicts the handheld imager assembly. All optical components are mounted to a single aluminum base plate (6.4 × 30 × 0.3 cm).

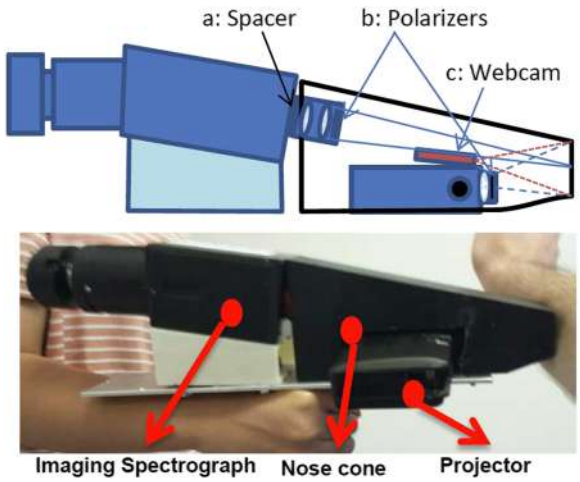

FIG. 3. Clinical imaging head: Top figure shows the imaging head schematic, identifying the (a) brass spacer that modifies the field of view and focal length of the standard 35 mm marco-lens, (b) locations of the crossed polarizers to reject specular reflection, and (c) the endoscopic webcam that localizes the relative positions of projector and slit imaging spectrograph, relative to the tissue. Bottom image depicts the physical device, indicating the relative placements of the imaging spectrograph to the projector and nose cone.

The projector was designed with a single ¼-20 mounting thread at its base. Through this thread, the projector is mounted directly to the aluminum base plate. This, however, only secures the projector to the base plate at a single point. To prevent any rotational misalignment of the projector, the nose cone of this system (described in more detail below) was designed to fit securely over the projection unit. The nose cone is secured via 8-32 thread screws to the base plate at four locations (2 in front and 2 behind the projector), thereby securing the projector in a fixed location and orientation.

Angled mounting brackets were fabricated via 3D printing with an 8° pitch. These brackets are secured by two 8-32 screws (each) to the base plate and the top of the brackets also aligns with the four mounting 8-32 tapped mounts at the base of the imaging spectrograph. Offset from the projector, these mounting brackets allow the imaging spectrometer to collect an image at a plane that is not only coincident with the projector's image plane but centered in the projector's field of view, given the bracket's height and angle.

4. Additional features

a. Rejection of specular reflection from tissue surface. Since the tissue volume of interest lies in the superficial subsurface, it is important to avoid collecting specular reflections from the skin surface. To address this, a cross-polarizer configuration is employed between the light output from the projector and the collection lens of the imaging spectrograph. A wire mesh polarizer is fixed to the distal end of the modified projection lens system, thereby only allowing linearly polarized light to reach the tissue. Additionally, a crossed polarizer was fixed to the front of the 35 mm lens system of the imaging spectrograph, rotated 90° relative to the polarizer on the illumination/projection unit. Figure 3 illustrates the placement of these polarizers.

b. Nose cone. A plastic enclosure was designed and fabricated that covers the light-paths from the projector to the tissue of interest and from that tissue to the imager. The cone is open at the end which is placed in contact with the skin during the imaging process. The nose cone was designed in SolidWorks 3D CAD 2015 (SOLIDWORKS, Waltham, MA) as a single piece and fabricated from Polylactic Acid (PLA) via 3D printing (FabWorks, University of California, Irvine).

This component serves several purposes to assist in the robust acquisition of SFDS data. One consequence of the compact design of the handheld imager is that both projection and imager optics have relatively short working distances. This results in a narrow depth of focus. As this is a co-planar imaging system, the positioning of the subject within the focal volume of both projector and imager is critical. By presenting a physical contact and a fixed distance, this nose cone ensures that the subject is within ~±1 mm of the focus of both the projector and imager. By maintaining tissues within this tight range of the ideal imaging plane, estimated errors due to defocus will contribute less than 2% of the determined absorption and scattering values.

Physical contact with tissues also minimizes any potential motion artifacts. It has been shown that motion is a big factor in introducing errors into spatial frequency domain imaging techniques. If left uncompensated, subject's movements will result in a large variance of the measured optical properties.[28] By keeping contact between the imager and tissue, the nose cone helps minimize motion artifacts to produce accurate optical properties, even when data acquisition times exceed the desired target acquisition time of <10 s.

Lastly, the nose cone helps block stray light. This allows us to acquire images in the presence of ambient room light, which is typically difficult to control in clinical exam rooms. The black material, from which the nose cone is fabricated, helps reduce the propagation of internally reflected stray light within the imaging head.

c. Webcam. Since the spectroscopy system only acquires image data along a single line, it is difficult to accurately visualize and identify where the line image data are being collected from the tissue. In order to assist the user with accurate positioning of the device with respect to a tissue region of interest, a simple video graphics array (VGA) webcam (2 m USB waterproof endoscope, VicTsing), stripped of its commercial housing, was placed next to the projection optics of this device (Fig. 3). Matching the working distance of the projection optics, this webcam can provide a 3-color 2D image of tissues across the entire fields of view of both the projector and spectral imager. With both the projector and spectral imager having a fixed, co-planar field of view, the webcam can overlay the location of where the imager collects the spectral data in relation to the region of tissues illuminated by the projector. At the start of every acquisition, this webcam image (with the software overlay of the spectral imager data collection) is automatically saved through our LabVIEW acquisition code, providing a documented reference of the spatial location from which imaging data were collected.

C. Software

1. Software control of the projector

Using a commercially available consumer grade projector limits the ability to directly control the full functionality of the DMD within the projector via software. Thus, we employ the projector as a second monitor to project a sequence of spatial frequency dependent patterns in the video mode. While any number of programming languages can generate codes to automatically project images through a second monitor (C#, Matlab, LabVIEW, etc.), these will be limited by the embedded firmware of the projector itself.

The first limitation of this approach is that consumer grade projectors are encoded to project color images at a typical frame rate of 30 Hz. For these LED driven projectors, the DMD produces 8-bit patterns at 90 Hz (3 LEDs are sequentially projected to form RGB images at a combined 30 Hz rate). Since we have replaced the LEDs with a steady state broadband light source, we have illumination at a rate of 90 Hz, but it will run asynchronously from our line imaging spectrometer. This limits the acquisition speed of this system to ~100 ms/pattern

to ensure that any artifacts resulting from a partial projection frame (<11 ms) are eliminated.

Additionally, video projections do not display images linearly across the dynamic range of the DMD. Monitors and projectors are tailored to the nonlinear response of human perception and hence convolve any input image with a gamma function, before projecting it.[29] In this case, if a purely sinusoidal intensity image were to be used as an input to the projector, the intensity distribution projected onto tissues would no longer be sinusoidal. We have characterized the intensity throughput function (gamma correction) for this specific projector by measuring the intensity of a series of grayscale planar images reflected from a known reflectance standard (SRT-99-100, Labsphere, North Sutton, NH) and used this to precondition every spatial frequency image used, ensuring that the resulting intensity pattern projected onto tissues will represent a pure sinusoid (Fig. 4).

2. System initialization and data acquisition

A graphical user interface (GUI) was developed using LabVIEW (National Instruments, Austin, TX) to manage the initialization of the individual components in the imager as well as to execute the image acquisition sequence. The GUI allows the user to specify the number and range of spatial frequencies to be used in the acquisition sequence. The program will then generate a sequence of gamma compensated images (Sec. II C 1) that covers the specified range of spatial frequencies in evenly spaced increments. Following the demodulation procedure that we have previously described,[7] three images are generated at even phase intervals [0°, 120°, 240°] at each spatial frequency that is employed. This enables the spatial frequency specific reflectance response to be demodulated at every pixel location. Once the imager has been positioned over the tissue region of interest, an auto-exposure routine is executed to determine the optimal integration time for the spectrograph while avoiding saturation of any pixels in the sensor. This auto-exposure feature requires <1 s to run.

When the acquisition sequence is initiated, the projector DMD is illuminated by the light source. Configured as a second monitor, the Optoma unit projects the modulated illumination in a window that fills the entire field of view of the projector. The imaging spectrograph then acquires data within the predefined integration time. Once the image acquisition is complete, the data are saved to a disk in an uncompressed format (TIFF) and the next image is sent to the projector. This sequence is repeated until all patterns are projected and spectral images are acquired.

Once data acquisition from the tissue region of interest is completed for any given subject, a reference calibration measurement is then acquired.[7] Here, the imager acquires spectral image data from a polydimethylsiloxane tissue simulating phantom with stable and rigorously characterized optical properties. We have described the fabrication of these phantoms in detail previously.[30,31] This step is performed using the same measurement parameters as the tissue measurement, thereby calibrating the tissue data at each spatial frequency directly.[7]

III. SYSTEM EVALUATION

In order to validate the performance of this imaging system, we first compare its performance to that of our benchtop point-spectroscopy SFDS system for the same homogeneous tissue simulating phantom.[30] The objective of this assessment is to demonstrate that the system presented here performs comparably to our reference system, independent of any depth sensitivity differences due to slight changes in measurement geometry.

In order to demonstrate both the spatial resolution and *in vivo* utility of the line imaging configuration, an example pigmented lesion was imaged *in vivo*. Though clinically benign, this example demonstrates that this imager is capable to measuring a wide range of spatially resolved optical properties, while maintaining sufficient dynamic range along both spatial and spectral dimensions. Additionally, because skin is a layered tissue, this comparison also indicates whether the

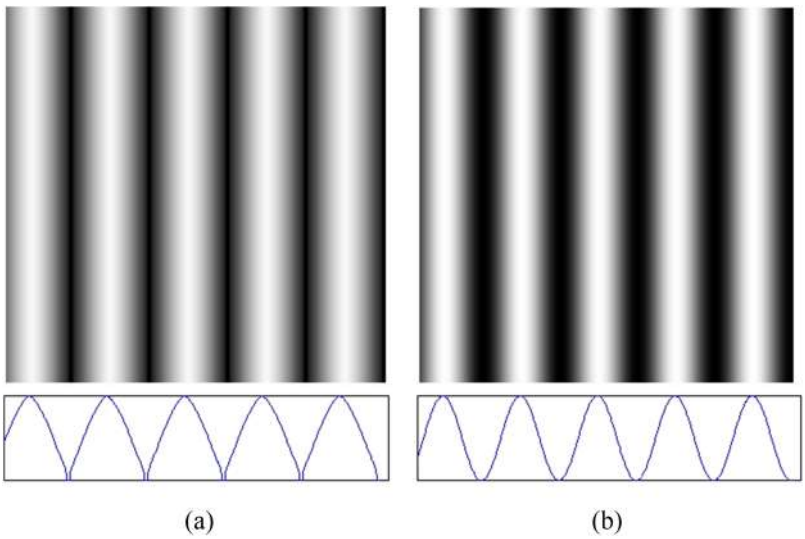

FIG. 4. Correcting for native gamma function in projector. (a) Input intensity pattern image sent to projector (pre-conditioned for gamma function) and (b) output pattern from projector (now sinusoidal in intensity across the lateral dimension). Bottom figures show the respective lateral (line-out) intensity functions.

measurement geometry of this new imager will be biased toward more superficial or deeper volumes of tissues, relative to the benchtop system.

A. Comparison using homogeneous tissue phantom

For this investigation, we used a homogeneous tissue simulating phantom that uses nigrosin as the absorbing agent and titanium oxide as the scattering agent.[30] Because nigrosin has strong absorption in the visible wavelength range but rolls off in the near infrared portion of the spectrum, this enables us to cover the broad range of absorption values anticipated in skin in a single sample. The system was set to use the same spatial frequencies (0, 0.05, 0.1, 0.15, 0.2 mm^{-1}) and phases (0, 120, 240). All data were processed the same way. Figure 5 shows the calibrated reflectance at all five spatial frequencies measured by both systems. Differences in calibrated demodulated reflectance between the two instruments were within 1% agreement. This resulted in differences of the absorption coefficient of <5%, on average. The difference between the calculated reduced scattering coefficient was <2%. The largest spectral differences were observed in 450-500 nm and 950-1000 nm wavelength bands. These differences also lie in spectral regions where the quantum efficiency is the lowest for the sensors used in these instruments, resulting in relatively low levels of light detected. Since the 450-500 nm region held more than a 10% disparity in absorption between systems, we have opted to only consider data acquired at wavelengths longer than 500 nm.

B. *In vivo* measurement

In vivo measurements of a clinically benign pigmented lesion were collected by both systems under an Institutional Review Board (IRB) approved protocol (UCI HS #2008-6307). Figure 6 illustrates data acquired from each.

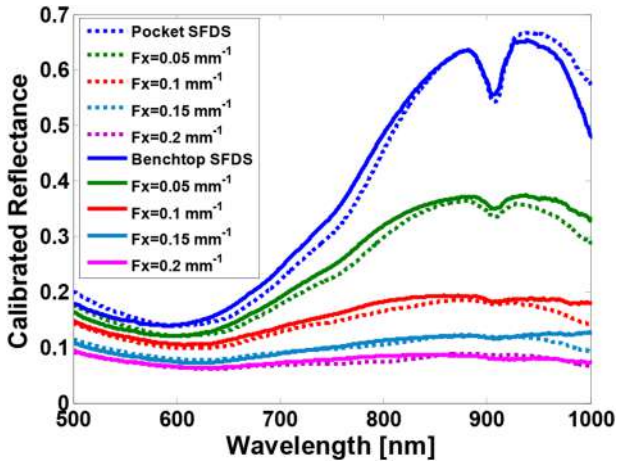

FIG. 5. Calibrated reflectance spectra from a nigrosin tissue simulating phantom at five spatial frequencies. The blue spectra are measured at 0 mm^{-1} spatial frequency (i.e., planar illumination) and the magenta spectra are measured at 0.2 mm^{-1}. Dotted lines are the mean spectra from the handheld imager; solid lines are from the benchtop system.

The benchtop system collected data from the center of the pigmented lesion and from normal skin adjacent to the right of the lesion. The handheld imager collected data from the same lesion (same orientation) transecting the lesion. It is also worth noting that, as the benchtop system performs a point-wise data collection, it can optimize the exposure time based on the reflectance at a single spatial location, while the line-imager limits the exposure time to the highest reflectance in the entire field of view. For this particular pigmented lesion, the benchtop system recorded the pigmented portion at an exposure time ~3× longer than that set for the normal adjacent skin. Also, these were serial measurements (co-registration accuracy ~1 mm) thus the sampling volumes are not the same (benchtop integrates over a 1 mm spot vs the handheld imager has a spatial resolution of ~300 μm). Figure 6 shows that the

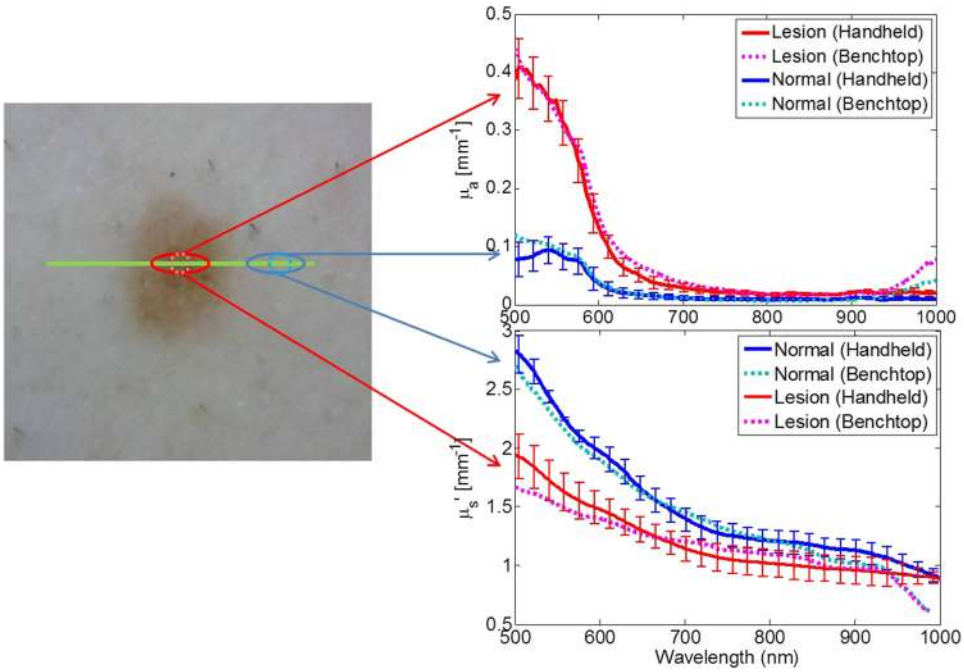

FIG. 6. *In vivo* measurement of a benign pigmented lesion. Left: Color image of lesion where the green line indicates where the handheld imager acquired the spatially resolved spectra. Red and blue solid lines represent the mean absorption (top right) and reduced scattering (bottom right) spectra measured by the handheld imager. The error bars indicate the spatial variance measured of the ellipses indicated on the left color image. Cyan and magenta spectra are the optical properties measured by the benchtop system at a single location from the center of the lesion and adjacent normal skin, respectively.

two instruments show strong agreement between each other in terms of both absorption and reduced scattering spectra, in spite of differences in the available dynamic range and precision of co-registration.

IV. DISCUSSION

We have designed and evaluated a handheld SFDS system utilizing commercially available consumer grade components. This novel, clinic-friendly imager enables *in vivo* study of skin. Our testing and validation have demonstrated that this instrument performs similarly to our benchtop system. It can project any number of spatial frequencies ranging between 0 and 0.5 mm^{-1}, with a spectral resolution of ~1 nm. The calibrated reflectance from known tissue simulating phantoms is within ~1% compared to that obtained for the same sample, measured using the benchtop system. This indicates that the calibrated spectral responses are very similar. The agreement between systems in the context of measuring both normal skin and a benign pigmented lesion suggests that the measurement geometry of both systems enables similar tissue interrogation volumes.

The 1D (one dimensional), line imaging system presented here has a number of advantages over the benchtop system. Among these advantages are superior portability and that it can simultaneously resolve spectral information using 1088 pixels along a line. In addition, the handheld system is based on relatively inexpensive components and the hardware for this was less than half the cost of the benchtop system hardware. The *in vivo* example demonstrates that the line-imager has sufficient dynamic range to measure both lightly and more heavily pigmented tissues simultaneously.

This new instrument is not without limitations. The most notable limitations are the size of the imager and the acquisition time. As our initial design criterion required 1 nm spectral resolution over a spectral range of 400-1000 nm, it is not the projector, webcam, nor the source that is a limiting factor of the imager size. The critical component is the means to provide spectrally resolved measurements over the range and resolution that we have specified. In the context of Vis/NIR 1 nm spectral imagers, there are limited options available. The BaySpec hyperspectral imager was the smallest unit available for purchase at the time that this fabrication was carried out. Smaller devices that we looked at during the design phase would have been an unsatisfactory compromise in terms of loss of wavelength coverage and resolution. This imager is limited in light throughput due to the 30 μm slit of the compact line imaging spectrograph. This results in total acquisition times on the order of 15-30 s when five spatial frequencies are used. This light throughput issue could be mitigated by replacing the entrance slit of spectrograph with a wider slit, trading off spectral resolution for light throughput. Once a deeper understanding of the spectral resolution requirements informed by the spectral variance and sensitivity of the initial study of pigmented lesions is determined, a wider replacement slit may be considered in order to leverage light throughput (acquisition speed) over spectral resolution. Alternatively, other more compact, hyperspectral imaging technologies may be considered (hyperspectral imagers manufactured by IMEC, Spectral Devices, Inc., etc.) should a broadening of spectral resolution and/or reduction of spectral range bare no significant consequence to the robust characterization of tissue properties in skin imaging.

Additionally, we have elected to acquire spectral responses from tissues at five spatial frequencies and utilize the standard three-phase demodulation method. This results in the acquisition of the remitted signal from 15 sequential illumination patterns. Alternatively, there are methods that could reduce total acquisition time by limiting the number of patterns projected. Single snapshot spatial frequency techniques simultaneously extract the spatial frequency and the unstructured (e.g., DC) component of the remitted light from a single projection pattern.[32] In this case, a single pattern can produce reflectance spectra at two spatial frequencies: 0 mm^{-1} and the spatial frequency at which the illumination is projected. Multi-frequency synthesis approaches utilize square-wave patterns for illumination instead of sinusoidal patterns.[24] The square wave illumination is modeled as a superposition of multiple sinusoidal spatial frequencies and hence allowing for more than two spatial frequencies to be extracted from a single pattern. While both approaches have the potential to significantly reduce acquisition time, extracting multiple spatial frequencies from a single pattern comes at the price of the reduced dynamic range and signal to noise ratio.

While the acquisition time may not be ideal, the total imaging session only requires less than 5 min of patient time and the physical contact of the imager's nose cone sufficiently manages any motion artifacts during the acquisition sequence. This handheld SFDS imager has the potential, never the less, to provide substantial insight into the visible and near infrared optical properties of a wide variety of dermatological pathologies without significantly impeding the clinical work flow.

V. CONCLUSION

Translating benchtop systems into clinical settings involves careful design considerations. Clinical settings typically involve limited space, time, and control of environment (including illumination). Under these constraints, we have developed a translational, research-grade SFDS device that can measure skin optical properties that compare favorably with those measured using our original SFDS instrument. The new instrument is compact, easy to use, and enables relatively rapid data collection from *in-vivo* skin. The instrument will enable investigational skin studies that are quantitative, depth specific, and spatially resolved in one dimension. This is a critical foundation to gain a better understanding of the structure and function of the mesoscopic qualities of pigmented skin lesions including melanoma, in terms of optical sources of contrast.

ACKNOWLEDGMENTS

We thankfully recognize support from the Beckman Foundation and the NIH, including No. P41EB015890 (A Biomedical Technology Resource) from NIBIB. The content is solely the responsibility of the authors and does not necessarily

represent the official views of the NIBIB or NIH. The purchase of hardware components was supported in part with funding provided under a *UC Irvine*, *Institute for Clinical and Translational Science Triumvirate grant*.

[1]A. Vogel and V. Venugopalan, "Mechanisms of pulsed laser ablation of biological tissues," Chem. Rev. **103**(2), 577–644 (2003).
[2]J. R. Mourant, J. P. Freyer, A. H. Hielscher, A. A. Eick, D. Shen, and T. M. Johnson, "Mechanisms of light scattering from biological cells relevant to noninvasive optical-tissue diagnostics," Appl. Opt. **37**(16), 3586–3593 (1998).
[3]H. Jonasson, I. Fredriksson, M. Larsson, and T. Stromberg, "Assessment of the microcirculation using combined model based diffuse reflectance spectroscopy and laser Doppler flowmetry," in *16th Nordic-Baltic Conference on Biomedical Engineering* (Springer, 2015), Vol. 48, pp. 52–54.
[4]M. Milanič, A. Bjorgan, M. Larsson, P. Marraccini, T. Strömberg, and L. L. Randeberg, "Hyperspectral imaging for detection of cholesterol in human skin," Proc. SPIE **9332**, 93320W (2015).
[5]J. Y. Lo, B. Yu, T. F. Kuech, and N. Ramanujam, "A compact, cost-effective diffuse reflectance spectroscopic imaging system for quantitative tissue absorption and scattering," Proc. SPIE **7890**, 78900B (2011).
[6]J. Liu, A. Li, A. E. Cerussi, and B. J. Tromberg, "Parametric diffuse optical imaging in reflectance geometry," IEEE J. Sel. Top. Quantum Electron. **16**(3), 555–564 (2010).
[7]D. J. Cuccia, F. Bevilacqua, A. J. Durkin, F. R. Ayers, and B. J. Tromberg, "Quantitation and mapping of tissue optical properties using modulated imaging," J. Biomed. Opt. **14**(2), 024012 (2009).
[8]F. Bevilacqua, A. J. Berger, A. E. Cerussi, D. Jakubowski, and B. J. Tromberg, "Broadband absorption spectroscopy in turbid media by combined frequency-domain and steady-state methods," Appl. Opt. **39**(34), 6498–6507 (2000).
[9]K. Terstappen, M. Suurkula, H. Hallberg, M. B. Ericson, and A. M. Wennberg, "Poor correlation between spectrophotometric intracutaneous analysis and histopathology in melanoma and nonmelanoma lesions," J. Biomed. Opt. **18**(6), 061223 (2013).
[10]S. Vyas, A. Banerjee, and P. Burlina, "Estimating physiological skin parameters from hyperspectral signatures," J. Biomed. Opt. **18**(5), 057008 (2013).
[11]D. Yudovsky and L. Pilon, "Retrieving skin properties from *in vivo* spectral reflectance measurements," J. Biophotonics **4**(5), 305–314 (2011).
[12]T. Stromberg, H. Karlsson, I. Fredriksson, and M. Larsson, "Experimental results using a three-layer skin model for diffuse reflectance spectroscopy," Proc. SPIE **8578**, 857834 (2013).
[13]B. Majaron, M. Milanic, and J. Premru, "Monte Carlo simulation of radiation transport in human skin with rigorous treatment of curved tissue boundaries," J. Biomed. Opt. **20**(1), 015002 (2015).
[14]D. Yudovsky, J. Q. M. Nguyen, and A. J. Durkin, "*In vivo* spatial frequency domain spectroscopy of two layer media," J. Biomed. Opt. **17**(10), 107006 (2012).
[15]A. Bjorgan, M. Milanic, and L. L. Randeberg, "Estimation of skin optical parameters for real-time hyperspectral imaging applications," J. Biomed. Opt. **19**(6), 066003 (2014).
[16]F. Vasefi, N. MacKinnon, R. Saager, K. M. Kelly, T. Maly, N. Booth, A. J. Durkin, and D. L. Farkas, "Separating melanin from hemodynamics in nevi using multimode hyperspectral dermoscopy and spatial frequency domain spectroscopy," J. Biomed. Opt. **21**(11), 114001 (2016).
[17]R. B. Saager, D. J. Cuccia, and A. J. Durkin, "Determination of optical properties of turbid media spanning visible and near-infrared regimes via spatially modulated quantitative spectroscopy," J. Biomed. Opt. **15**(1), 017012 (2010).
[18]R. B. Saager, A. Sharif, K. M. Kelly, and A. J. Durkin, "*In vivo* isolation of the effects of melanin from underlying hemodynamics across skin types using spatial frequency domain spectroscopy," J. Biomed. Opt. **21**(5), 057001 (2016).
[19]R. B. Saager, A. Truong, D. J. Cuccia, and A. J. Durkin, "Method for depth-resolved quantitation of optical properties in layered media using spatially modulated quantitative spectroscopy," J. Biomed. Opt. **16**(7), 077002 (2011).
[20]R. B. Saager, M. Balu, V. Crosignani, A. Sharif, A. J. Durkin, K. M. Kelly, and B. J. Tromberg, "*In vivo* measurements of cutaneous melanin across spatial scales: Using multiphoton microscopy and spatial frequency domain spectroscopy," J. Biomed. Opt. **20**(6), 066005 (2015).
[21]S. A. Carp, S. A. Prahl, and V. Venugopalan, "Radiative transport in the delta-P1 approximation: Accuracy of fluence rate and optical penetration depth predictions in turbid semi-infinite media," J. Biomed. Opt. **9**(3), 632–647 (2004).
[22]S. L. Jacques, "Optics of light dosimetry for PDT in superficial lesions versus bulky tumors," Proc. SPIE **4612**, 59–68 (2002).
[23]D. J. Rohrbach, D. Muffoletto, J. Huihui, R. Saager, K. Keymel, A. Paquette, J. Morgan, N. Zeitouni, and U. Sunar, "Preoperative mapping of nonmelanoma skin cancer using spatial frequency domain and ultrasound imaging," Acad. Radiol. **21**(2), 263–270 (2014).
[24]K. P. Nadeau, T. B. Rice, A. J. Durkin, and B. J. Tromberg, "Multifrequency synthesis and extraction using square wave projection patterns for quantitative tissue imaging," J. Biomed. Opt. **20**(11), 116005 (2015).
[25]A. J. Lin, A. Ponticorvo, S. D. Konecky, H. T. Cui, T. B. Rice, B. Choi, A. J. Durkin, and B. J. Tromberg, "Visible spatial frequency domain imaging with a digital light microprojector," J. Biomed. Opt. **18**(9), 096007 (2013).
[26]R. B. Saager, D. J. Cuccia, S. Saggesse, K. M. Kelly, and A. J. Durkin, "A LED based spatial frequency domain imaging system for optimization of photodynamic therapy of basal cell carcinoma (BCC)," Lasers Surg. Med. **43**, 917 (2011).
[27]A. Breslow, "Thickness, cross-sectional areas and depth of invasion in the prognosis of cutaneous melanoma," Ann. Surg. **172**(5), 902–908 (1970).
[28]J. Q. Nguyen, R. B. Saager, D. J. Cuccia, K. M. Kelly, J. Jakowatz, D. Hsiang, and A. J. Durkin, "Effects of motion on optical properties in the spatial frequency domain," J. Biomed. Opt. **16**(12), 126009 (2011).
[29]C. A. Poynton, *Digital Video and HDTV: Algorithms and Interfaces*, Morgan Kaufmann Series in Computer Graphics and Geometric Modeling (Morgan Kaufmann Publishers, Amsterdam, Boston, 2003), Chap. xlii, p. 692.
[30]F. Ayers, A. Grant, D. Kuo, D. J. Cuccia, and A. J. Durkin, "Fabrication and characterization of silicone-based tissue phantoms with tunable optical properties in the visible and near infrared domain," Proc. SPIE **6870**, 687007 (2008).
[31]R. B. Saager, C. Kondru, K. Au, K. Sry, F. Ayers, and A. J. Durkin, "Multilayer silicone phantoms for the evaluation of quantitative optical techniques in skin imaging," Proc. SPIE **7567**, 756706 (2010).
[32]J. Vervandier and S. Gioux, "Single snapshot imaging of optical properties," Biomed. Opt. Express **4**(12), 2938–2944 (2013).